

The hadronic light by light contribution to the $(g - 2)_\mu$ with holographic models of QCD

Luigi Cappiello^{1,2}, Oscar Catà³ and Giancarlo D'Ambrosio²

¹*Dipartimento di Scienze Fisiche, Università di Napoli "Federico II", Via Cintia, 80126 Napoli, Italy*

²*INFN-Sezione di Napoli, Via Cintia, 80126 Napoli, Italy and*

³*Departament de Física Teòrica and IFIC, Universitat de València-CSIC, Apt. Correus 22085, E-46071 València, Spain*

We study the anomalous electromagnetic pion form factor $F_{\pi^0\gamma^*\gamma^*}$ with a set of holographic models. By comparing with the measured value of the linear slope, some of these models can be ruled out. From the remaining models we obtain predictions for the low-energy quadratic slope parameters of $F_{\pi^0\gamma^*\gamma^*}$, currently out of experimental reach but testable in the near future. We find it particularly useful to encode this low-energy information in a form factor able to satisfy also QCD short-distance constraints. We choose the form factor introduced by D'Ambrosio, Isidori and Portoles in kaon decays, which has the right short distance for a particular value of the quadratic slope, which is later shown to be compatible with our holographic predictions. We then turn to a determination of the (dominant) pion exchange diagram in the hadronic light by light scattering contribution to the muon anomalous magnetic moment. We quantify the theoretical uncertainty in $(g - 2)_\mu$ coming from the different input we use: QCD short distances, experimental input and low-energy holographic predictions. We also test the pion-pole approximation. Our final result is $a_\mu^{\pi^0} = 6.54(25) \cdot 10^{-10}$, where the error is driven by the linear slope of $F_{\pi^0\gamma^*\gamma^*}$, soon to be measured with precision at KLOE-2. Our numerical analysis also indicates that large values of the magnetic susceptibility χ_0 are disfavored, therefore pointing at a mild effect from the pion off-shellness. However, in the absence of stronger bounds on χ_0 , an additional $(10 - 15)\%$ systematic uncertainty on the previous value for $a_\mu^{\pi^0}$ cannot be excluded.

PACS numbers: 14.60.Ef, 13.40.Em, 11.25.Tq

I. INTRODUCTION

The anomalous magnetic moment of the muon is presently one of the most stringent tests of the standard model and, due to the current experimental precision, a very useful tool in the search for new physics. As of today, a discrepancy of roughly three standard deviations persists between the standard model estimate and the experimental value at Brookhaven [1]. Whether this is to be ascribed to evidence for new physics depends crucially on the reliability of the standard model computation.

With the electroweak corrections under good control, the main source of uncertainty on the theoretical side comes from the hadronic contributions, namely the vacuum and the light-by-light contributions. While information on the hadronic vacuum polarization can be extracted from experimental data on the hadronic e^+e^- cross section, the hadronic light-by-light (HLBL) contribution can only be estimated through nonperturbative theoretical methods, *i.e.* lattice simulations and hadronic models. Due to the complexity of the calculation, a lattice result is unfortunately still not available and one has to resort to the latter.

In the past there have been plenty of determinations based on particular models like the ENJL [2], HLS [3] and more recently on different models in-

spired by the $1/N_c$ expansion under the assumption of lowest meson dominance (LMD) [4–6]. Different as they are in nature, all the abovementioned models eventually determine their free parameters imposing constraints, either theoretical or experimental. Therefore, the source of uncertainty generally depends on: (i) the experimental input used; (ii) the different theoretical constraints imposed; and (iii) an intrinsic model dependence, which is very difficult to estimate. While it is certainly reassuring that, ever since the seminal paper of Ref. [7] settled an important sign issue, the results for the different models lie in the same ballpark and no big disagreement is present, there are certain unresolved issues that might affect the theoretical error estimate (see for instance the recent discussion in [8]). With the proposals at Fermilab [9], J-PARC [10] and potentially at Frascati [11], the increase in experimental precision will aim at reaching $1.5 \cdot 10^{-10}$ accuracy. Therefore, a reliable estimate of the theoretical error in the hadronic light-by-light contribution becomes of the utmost importance (see, for instance, the recent assessments of the error budget given in Refs. [12, 13]).

In this paper we propose to use the holographic principle [14] to address such issues. Holographic models of QCD, while also based on the $1/N_c$ expansion, offer several advantages over four-dimensional LMD models. First and foremost, AdS/QCD mod-

els are implemented at the Lagrangian level, and therefore Ward identities between correlators are automatically fulfilled. Second, due to the AdS metric, short-distance matching to asymptotically free QCD is easily achieved. Third, hadronic resonances in AdS/QCD models arise as the Kaluza-Klein states in the process of compactification from five to four dimensions. Therefore, as opposed to LMD models, the full tower of states is automatically implemented and its separate contributions can be analyzed. Finally, even though an infinite number of resonances is present, the number of free parameters is very small. Thus, unlike phenomenological hadronic models, very little input is needed in order to be predictive. Holography, therefore, has the potential to become a consistent hadronic model for all the hadronic light-by-light contributions to $(g-2)_\mu$, at least at leading order in the $1/N_c$ expansion, *i.e.*, in the limit of single-resonance exchange.

In this paper we will concentrate on the neutral pion exchange contribution. Traditionally, this contribution has been extracted from the knowledge on the electromagnetic pion form factor $F_{\pi^0\gamma^*\gamma^*}$. The questions we want to address are the following:

- (i) Which are the parameters entering $F_{\pi^0\gamma^*\gamma^*}$ that mostly affect the uncertainty on $(g-2)_\mu$?
- (ii) It has been recently pointed out [15] that the quadratic slope $\hat{\beta}$, defined by

$$\lim_{Q_1^2, Q_2^2 \rightarrow 0} F_{\pi^0\gamma^*\gamma^*}(Q_1^2, Q_2^2) \simeq -\frac{N_C}{12\pi^2 f_\pi} \times \left[1 + \hat{\alpha} (Q_1^2 + Q_2^2) + \hat{\beta} Q_1^2 Q_2^2 + \hat{\gamma} (Q_1^4 + Q_2^4) + \dots \right]$$

might be of importance to reduce the uncertainty in the $(g-2)_\mu$. However, an experimental determination thereof is still lacking. Can holographic models of QCD be used to estimate the linear and quadratic slopes of $F_{\pi^0\gamma^*\gamma^*}$? Do these models satisfy the required short-distance constraints? How big is the impact of the holographic slopes on $(g-2)_\mu$?

- (iii) Is vector-meson dominance a justified approximation for $F_{\pi^0\gamma^*\gamma^*}$? How does this approximation carry over to the evaluation of the $(g-2)_\mu$?
- (iv) What is the impact of not restricting the neutral pion to be on-shell in the HLBL contribution? In other words, what is the accuracy of the pion-pole approximation?

In order to address these questions we will study $F_{\pi^0\gamma^*\gamma^*}$ in a set of holographic models, which mostly differ in the way they implement chiral symmetry breaking and the spacing in the hadronic vector

spectrum (Regge-like or not). We will test the models against existing experimental data on $F_{\pi^0\gamma^*\gamma^*}$. In particular, we will compare the different predictions for the linear slope $\hat{\alpha}$ with the results from CELLO [16]. Agreement with experiment will be used as a filtering criteria for the different models. Then, from the accepted models, we will extract a prediction for the quadratic slopes $\hat{\beta}$ and $\hat{\gamma}$.

For the analysis of the $(g-2)_\mu$ we will adopt a strategy similar in spirit to Ref. [17], where a set of simple interpolators were tested against experiment and then used to estimate the contribution to the HLBL. A particularly useful form factor, which displays immediately the required short and long-distance properties is found to be the one used by D'Ambrosio, Isidori and Portoles (DIP) in kaon decays [18]:

$$K(q_1^2, q_2^2) = 1 + \lambda \left(\frac{q_1^2}{q_1^2 - m_V^2} + \frac{q_2^2}{q_2^2 - m_V^2} \right) + \eta \frac{q_1^2 q_2^2}{(q_1^2 - m_V^2)(q_2^2 - m_V^2)}.$$

In particular, to study the pion off-shellness we will promote the DIP form factor to an interpolator valid for arbitrary pion momentum. This leads to a new short-distance constraint [6] which is naturally implemented in our DIP interpolator.

This paper is organized as follows: in Section II we will briefly review the holographic principle and its most common realizations to study QCD. These models will then be used in Section III to study the $\pi^0\gamma^*\gamma^*$ form factor, with special emphasis on its low-energy predictions. In Section IV we will introduce the DIP interpolator and i) give a first estimate of the pion exchange contribution to the HLBL piece of $(g-2)_\mu$ and then ii) present an extension of the DIP interpolator with an extra pole, which will allow us to play with the whole set of long and short-distance constraints and test the stability of our results. Finally, conclusions will be given in Section V. Technical details are provided in two Appendices. The paper is organized such that readers interested in phenomenological applications can skip Section II without loss of continuity.

II. HOLOGRAPHIC MODELS OF QCD

The AdS/CFT conjecture [14] offers one of the most promising ways to study gauge theories in strongly coupled regimes through their weakly coupled supergravity duals compactified in AdS_5 . In the recent years attempts have been directed towards using the gauge/string duality to QCD, *i.e.*, a holographic equivalence is conjectured between four-dimensional strongly coupled QCD at large N_c

and a five-dimensional weakly interacting gauge theory coupled to gravity on a five-dimensional space not necessarily (but asymptotically) AdS_5 . The fact that QCD is conformally invariant in the deep Euclidean makes the gauge/string duality a good starting point towards a theory of hadrons. However, QCD is not conformal in the strongly coupled regime and crucial ingredients like confinement or chiral symmetry breaking have to be incorporated. Confinement can be easily modeled by making the bulk space compact, for instance by placing an infrared brane some distance z_0 away from the ultraviolet brane. The QCD resonances are then the Kaluza-Klein modes arising from the compactification. Chiral symmetry breaking is more involved but AdS/CFT seems to have the potential to describe both explicit and spontaneous symmetry breaking [19]. The pion field can also be incorporated, and the agreement of the whole picture with QCD, especially with vector mesons, is quite remarkable [20–23].

In order to bridge the gap between the original AdS/CFT conjecture and AdS/QCD two main approaches have been followed, the so-called top-down and bottom-up. In the top-down approach, one looks for a suitable setting of D-branes in string theory, with gauge theory on their world volume, which at low energy would produce an effective background geometry for the dual five-dimensional gravitational theory. An example is the Sakai-Sugimoto model [22] to be considered later.

The bottom-up approach is more phenomenologically oriented and one starts directly from warped five-dimensional models, with an AdS_5 metric in the ultraviolet regime but with drastic deviations in the infrared, where nonperturbative effects of QCD force a description in terms of new low-energy degrees of freedom. In this paper we will consider Hard-Wall (HW) and Soft-Wall (SW) models. Both in the HW models of [20] and [24], the AdS_5 space is cut off at a finite size, producing an infinite number of Kaluza-Klein resonances, to be identified with the hadronic

spectrum. The two models differ in the implementation of χSB , though. In [20], χSB is induced by a 5D scalar field, holographically dual of the $\bar{q}q$ operator of QCD, whose nonvanishing vacuum expectation value is responsible for χSB . In contrast, in [24], χSB is achieved by imposing appropriate infrared boundary conditions. The SW model proposed in [25] is a five-dimensional holographic model in which the AdS_5 space is noncompact. Confinement and an infinite number of bound states follow from the presence of a nontrivial dilaton background. The main feature of the SW model is its ability to produce an hadronic spectrum with Regge behavior, which leads to better agreement with the resonance spectrum in QCD.

In any of the models above, one boldly conjectures the applicability of the holographic recipe to compute correlation functions of the dual 4-dimensional theory [26, 27]. For every quantum operator $\mathcal{O}(x)$ in QCD, there exists a corresponding bulk field $\phi(x, z)$, whose value on the ultraviolet brane, $\phi(x, 0) \equiv \phi_0(x)$, is identified with the four-dimensional source of $\mathcal{O}(x)$. Hence, the generating functional of the four-dimensional theory can be computed from the five-dimensional action evaluated *on-shell* (neglecting stringy corrections), *i.e.*,

$$\exp(iS_5[\phi_0(x)]) = \langle \exp \left[i \int d^4x \phi_0(x) \mathcal{O}(x) \right] \rangle_{\text{QCD}_4} . \quad (1)$$

Integrating by parts the quadratic part of the five-dimensional action on-shell effectively reduces to a boundary four-dimensional term quadratic in $\phi_0(x)$. By varying the action with respect to $\phi_0(x)$ one can generate the different connected n -point Green's functions of QCD.

The simplest five-dimensional action can be generically written in the form

$$S_5 = S_{\text{YM}} + S_X + S_{\text{CS}} , \quad (2)$$

where

$$\begin{aligned} S_{\text{YM}} &= -\text{tr} \int d^4x \int_0^{z_0} dz e^{-\Phi(z)} \frac{1}{8g_5^2} w(z) \left[\mathcal{F}_{(L)}^{MN} \mathcal{F}_{(L)MN} + \mathcal{F}_{(R)}^{MN} \mathcal{F}_{(R)MN} \right] , \\ S_X &= \text{tr} \int d^4x \int_0^{z_0} dz e^{-\Phi(z)} w(z)^3 \left[D^M X D_M X^\dagger + V(X^\dagger X) \right] , \end{aligned} \quad (3)$$

with $\mathcal{F}_{MN} = \partial_M \mathcal{B}_N - \partial_N \mathcal{B}_M - i[\mathcal{B}_M, \mathcal{B}_N]$ and $\mathcal{B}_{L,R} = V \mp A$, where $V(A) \in U(2)_{V(A)}$ are vector (axial-

vector) five-dimensional fields. If these are coupled to Dirac currents, then the holographic prescription

predicts that they are massless and hence gauge-invariant. It is common to work in the axial gauge $V_5 = A_5 = 0$. The surviving five-dimensional gauge fields $V_\mu(x, z)$ and $A_\mu(x, z)$ holographically correspond to four-dimensional vector and axial-vector QCD currents, $\bar{q}\gamma_\mu q$ and $\bar{q}_R\gamma_\mu\gamma_5 q_R$, respectively.

$\Phi(z)$ is a dilaton field and $X(x, z)$ a scalar field transforming under the chiral group as $g_L X g_R^\dagger$. Then, accordingly, $D_M X = \partial_M X - iL_M X + iX R_M$. As we shall see below, the presence of the scalar field X and the form of its potential depend on the model considered. For instance, in models where χ SB is induced by chirally-asymmetric boundary conditions on the gauge fields, $X(x, z)$ is not essential.

The extra-dimension is taken to extend over the interval $(0, z_0)$, where the upper limit can be infinite for some models. The metric of the five-dimensional space can be written generically in terms of a warp factor $w(z)$ as

$$g_{MN} dx^M dx^N = w(z)^2 (\eta_{\mu\nu} dx^\mu dx^\nu - dz^2) , \quad (4)$$

where $\eta_{\mu\nu} = \text{Diag}(1, -1, -1, -1)$, $\mu, \nu = (0, 1, 2, 3)$ and $M, N = (0, 1, 2, 3, z)$. In AdS_5 space the warping factor takes the form $w(z) = 1/z$.

As pointed out in [28], anomalous processes in four dimensions can be reproduced from the five-dimensional Chern-Simons term

$$S_{\text{CS}}[\mathcal{B}] = \frac{N_c}{24\pi^2} \int \text{tr} \left(\mathcal{B} \mathcal{F}^2 - \frac{i}{2} \mathcal{B}^3 \mathcal{F} - \frac{1}{10} \mathcal{B}^5 \right) . \quad (5)$$

In order to account for chirality, one should work with

$$S_{\text{CS}}^{\text{AdS}}[\mathcal{B}_L, \mathcal{B}_R] = S_{\text{CS}}[\mathcal{B}_L] - S_{\text{CS}}[\mathcal{B}_R] . \quad (6)$$

In the following we will briefly review the general features of the holographic models we will consider for our analysis of the electromagnetic pion form factor, mainly to fix our notation. Further details can be found in the original literature.

A. Hard-Wall models

The distinguishing features of HW models are a compact fifth dimension, $0 \leq z \leq z_0$ and a constant dilaton field $\Phi(z)$. We will concentrate on two such models, which we name HW1 [20, 21] and HW2 [24]. The presence of the upper bound $z = z_0$ defines an infrared brane, producing an explicit breaking of the scale invariance of the dual four-dimensional theories at energies $\approx 1/z_0 \approx 1$ GeV. Moreover, in the presence of this cutoff, Wilson loops follow an area-law behavior in the infrared regime, thereby simulating the onset of a confining phase.

In compliance with χ SB in the four-dimensional theory, axial gauge invariance is broken in the five-dimensional background, the longitudinal component of the axial-vector field becoming physical and related to the pion field.

HW1 and HW2 differ in the mechanism leading to the χ SB. In the HW1 model, the breaking is due to the scalar field $X(x, z)$, whose coupling to the axial-vector gauge field produces an effective mass term, breaking the gauge invariance in the axial sector. In the HW2 model, instead, no such field is present in the five-dimensional Lagrangian (2) and χ SB is achieved through different infrared boundary conditions for vector and axial-vector fields.

1. χ SB from a scalar bulk field: HW1

One considers the action (3) without dilaton field and with the complex scalar field $X(x, z) = v(z)U(x, z)/2$, where U contains the pion field and $v(z)$ is the scalar component that breaks chiral symmetry in the bulk. The scalar potential is reduced to the mass term, given by:

$$V(X^\dagger X) = \frac{3}{z^5} X^\dagger X . \quad (7)$$

The previous expression guarantees that X can be coupled to $\bar{q}q$. Solving the five-dimensional equations of motion at zero four-dimensional momentum one finds $v(z) = (m_q z + \sigma z^3)$, where the parameters m_q and σ are holographically identified as the quark mass and the $\bar{q}q$ condensate, *i.e.* the sources of explicit and spontaneous χ SB, respectively.

A nonvanishing $v(z)$ induces a z -dependent mass term for the axial-vector field in Eq. (3), thereby breaking the degeneracy between vector and axial-vector resonances. The scalar field X also produces a nontrivial coupling between the longitudinal component of the axial-vector field and the pion field. Defining $A_{\mu\parallel}^a(q, z) = -iq_\mu \varphi(q, z)$ and $U(x, z) = \exp[2it^a \pi^a(x, z)]$ (for $SU(2)$, $t^a = \sigma^a/2$, with σ^a being the Pauli matrices) one gets the system of coupled equations [20]:

$$\partial_z \left(\frac{1}{z} \partial_z \varphi^a \right) + \frac{g_5^2 v(z)^2}{z^3} (\pi^a - \varphi^a) = 0 , \quad (8)$$

$$-q^2 \partial_z \varphi^a + \frac{g_5^2 v(z)^2}{z^2} \partial_z \pi^a = 0 . \quad (9)$$

As a result, the HW1 model satisfies the Gell-Mann–Oakes–Renner (GMOR) relation [29]:

$$m_\pi^2 f_\pi^2 = (m_u + m_d) \langle \bar{q}q \rangle = 2m_q \sigma . \quad (10)$$

The pion wave function $\varphi(z) = 1 - \Psi(z)$ can be obtained from the coupled equations (8) and (9) which

describe the dynamics in the axial sector. In the chiral limit, $m_q = 0$, one obtains

$$\Psi(z) = \Gamma[2/3] \left(\frac{\xi z^3}{2} \right)^{\frac{1}{3}} \left[I_{-1/3}(\xi z^3) - \frac{I_{2/3}(\xi z_0^3)}{I_{-2/3}(\xi z_0^3)} I_{1/3}(\xi z^3) \right], \quad (11)$$

where $\xi \equiv g_5 \sigma / 3$, σ being the quark condensate. The pion wave function is different from zero on the infrared brane,

$$\Psi(z_0) = \frac{\sqrt{3} \Gamma[2/3]}{\pi I_{-2/3}(\xi z_0^3)} \left(\frac{1}{2(\xi z_0^3)^2} \right)^{1/3}, \quad (12)$$

a fact that will be important in the evaluation of the anomalous amplitude.

By solving the equation of motion for the vector field ($Q^2 = -p^2$ being the 4-dimensional Euclidean momentum):

$$\partial_z \left(\frac{1}{z} \partial_z \mathcal{J} \right) - \frac{Q^2}{z} \mathcal{J} = 0, \quad (13)$$

subject to the (Dirichlet) ultraviolet boundary condition $\mathcal{J}(Q, 0) = 1$ and the (Neumann) infrared one, $\partial_y \mathcal{J}(Q, z_0) = 0$, one finds the so-called vector bulk-to-boundary propagator $\mathcal{J}(Q, z)$, which can be written in terms of Bessel functions:

$$\mathcal{J}(Q, z) = Qz \left[K_1(Qz) + I_1(Qz) \frac{K_0(Qz_0)}{I_0(Qz_0)} \right]. \quad (14)$$

Vector resonances are associated with solutions $\psi_n(z)$ of the equation of motion for the vector field at discrete $p^2 = m_n^2$, with vanishing boundary conditions: $\psi_n(0) = 0$, and $\partial_z \psi_n(z_0) = 0$.

2. χ SB through boundary conditions: HW2

The action of the HW2 model [24] is entirely given by the gauge field part of eq.(3). The role of the scalar field X as the source of chiral symmetry breaking is played by asymmetric boundary conditions between vector and axial fields. In this model, vectors are required to obey infrared Neumann boundary conditions while axial fields satisfy Dirichlet boundary conditions. This leads to a splitting in the mass spectra that qualitatively reproduces what is observed in nature.

The pion field is built from Wilson lines extending between the 5D boundaries:

$$U(x) = \xi_R(x) \xi_L^{-1}(x), \quad (15)$$

where

$$\xi_{L,R}(x) = P \exp \left\{ -i \int_0^{z_0} dz' \mathcal{B}_z^{L,R}(x, z') \right\}. \quad (16)$$

The fact that the pion is a nonlocal object leads to difficulties to implement the GMOR relation. For our purposes, this will not be of relevance, since we shall consider the HW2 model only in the chiral limit of massless pions.

Chiral symmetry breaking is implemented by splitting the fields like

$$\hat{V}_\mu(x, z) \equiv V_\mu(x, z) + \hat{V}_\mu(x, 0), \quad (17)$$

$$\hat{A}_\mu(x, z) \equiv A_\mu(x, z) + \alpha(z) \hat{A}_\mu(x, 0),$$

where the last terms are the sources and $\alpha(z)$, which plays the role of the pion wave function, is determined by demanding no mixing between the pion and the axial resonances:

$$\alpha(z) = 1 - \frac{z^2}{z_0^2}. \quad (18)$$

For comparison, we will also consider the flat case, *i.e.* $w(z) = 1$. In that case the bulk-to-boundary propagator takes the form

$$\mathcal{J}(Q, z) = \cosh(Qz) + \tanh(Qz_0) \sinh(Qz), \quad (19)$$

and the pion wave function is given by

$$\alpha(z) = 1 - \frac{z}{z_0}. \quad (20)$$

3. The Sakai-Sugimoto as an HW2 model

The original action of [22] is

$$S = S_{\text{YM}} + S_{\text{CS}}, \quad (21)$$

with

$$S_{\text{YM}} = -\kappa \int d^4x \int_{-\infty}^{\infty} dz \operatorname{tr} \left[\frac{1}{2} h(z) \mathcal{F}_{\mu\nu}^2 - k(z) \mathcal{F}_{\mu z}^2 \right], \quad (22)$$

where the functions $h(z)$ and $k(z)$ are given by

$$h(z) = (1 + z^2)^{-1/3}; \quad k(z) = 1 + z^2, \quad (23)$$

and S_{CS} is given in Eq. (6).

The constant κ is related to the 't Hooft coupling λ and the number of colors N_c as

$$\kappa = \frac{\lambda N_c}{216\pi^3}. \quad (24)$$

The model also has a mass scale M_{KK} which in (22) was absorbed in the dimensionless parameter z . For our numerical analysis, the two parameters will be chosen as [22]

$$M_{KK} = 949 \text{ MeV}, \quad \kappa = 0.00745, \quad (25)$$

in order to fit the experimental values of the ρ meson mass, $m_\rho \simeq 776$ MeV, and the pion decay constant, $f_\pi \simeq 92.4$ MeV.

The action (21) was obtained in [22] as the effective action of N_f probe D8-branes placed in the background of N_c D4-branes, studied in [30], and stands for an effective theory of mesons in four-dimensional (large N_c) QCD with N_f massless quarks. In the following we will reformulate the Sakai-Sugimoto model and show that it can be cast in the form of a HW2 model. This reformulation will prove useful for computational purposes in the following Section.

As a first step, let us define $y = \tan^{-1} z$, with values in the finite interval $-\pi/2 \leq y \leq \pi/2$, whose end points $y = \pm\pi/2$ correspond to the ultraviolet branes while the point $y = 0$ corresponds to the infrared brane. In the $A_z = 0$ gauge, (22) becomes

$$S_{\text{YM}} = -\kappa \int d^4x \int_{-\pi/2}^{\pi/2} dy \operatorname{tr} \left[\frac{1}{2} \tilde{h}(y) \mathcal{F}_{\mu\nu}^2 - \mathcal{F}_{\mu y}^2 \right], \quad (26)$$

where $\tilde{h}(y)$ is an *even* function of y . This allows us to decompose the gauge field \mathcal{A}_μ in parity-even and parity-odd parts as $\mathcal{A}_\mu = V_\mu + A_\mu$, with $V_\mu(x, -y) = V_\mu(x, y)$ and $A_\mu(x, -y) = -A_\mu(x, y)$, and restrict the theory to half the interval, *i.e.* $0 \leq y \leq \pi/2$. Parity transformations in the fifth dimension correspond to the exchange of left and right-handed chiralities and can be used to distinguish between vectors and axial-vector fields (vectors and axial-vectors having even and odd y -profiles, respectively). As a consequence, they satisfy different boundary conditions on the infrared brane (at $y = 0$), *i.e.* Neumann for vectors, $\partial_y V_\mu|_{y=0} = 0$, and Dirichlet $A_\mu|_{y=0} = 0$ for axial-vectors.

Next, let us define the dimensionless variable $z \equiv \pi/2 - y$, with $0 \leq z \leq \pi/2$ (not to be confused with the original variable in (22)). $z = 0$ corresponds to the ultraviolet brane and $z = \pm\pi/2$ to the infrared brane, and the action takes the following form:

$$S_{\text{YM}} = -\kappa \int d^4x \int_0^{\pi/2} dz \operatorname{tr} \left\{ (\sin z)^{-4/3} \times [(V_{\mu\nu} - i[A_\mu, A_\nu])^2 + (D_\mu A_\nu - D_\nu A_\mu)^2] - 2(\partial_z V_\mu)^2 - 2(\partial_z A_\mu)^2 \right\}, \quad (27)$$

where $V_{\mu\nu} = \partial_\mu V_\nu - \partial_\nu V_\mu - i[V_\mu, V_\nu]$ and $D_\mu A_\nu = \partial_\mu A_\nu - i[V_\mu, A_\nu]$.

In the new variable $z \in [0, \pi/2]$ the SS model takes the form of the HW2 model with different boundary conditions for vector and axial-vector fields on the infrared boundary $z = \pi/2$, and an effective metric which is not AdS₅:

$$g_{MN} dx^M dx^N = (\sin z)^{-\frac{4}{3}} \eta_{\mu\nu} dx^\mu dx^\nu - (\sin z)^{-\frac{8}{3}} dz^2. \quad (28)$$

The chiral field containing the pion is also built from Wilson lines extending between boundaries. One can easily show that in the SS model the function $\alpha(z)$ discussed in the previous subsection takes the simple form

$$\alpha(z) = 1 - \frac{2z}{\pi}. \quad (29)$$

Vector (and axial-vector) fields can be obtained by solving the bulk-to-boundary differential equation

$$\left(\frac{d^2}{dz^2} - \frac{Q^2}{(\sin z)^{4/3}} \right) \mathcal{J} = 0, \quad (30)$$

subject to the boundary conditions $\mathcal{J}_{V,A}(Q, 0) = 1$, and $\partial_z \mathcal{J}_V(Q, \pi/2) = 0$, $\mathcal{J}_A(Q, \pi/2) = 0$, for which there is no analytic expression. In Fig. 1 we show the first three normalized eigenfunctions for vector and axial-vector fields in the new extra-dimensional variable z . As usual, the Fourier transform of

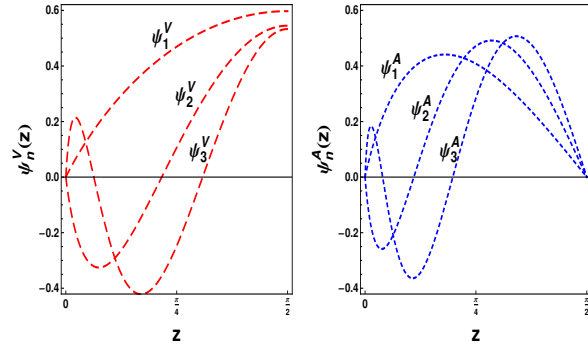


FIG. 1: The first three vector and axial-vector meson resonances of the SS model, using the new variable $z \in [0, \pi/2]$.

the five-dimensional gauge field has been written as $\mathcal{A}_\mu(q, z) = \tilde{\mathcal{A}}_\mu(q) \psi(z)$, with $\psi(z)$ satisfying the equation

$$\psi(z)'' + \frac{q^2}{(\sin z)^{4/3}} \psi(z) = 0. \quad (31)$$

Dynamical resonances $\psi_n(z)$ then correspond to normalized solutions of (31) with $q^2 = m_n^2$, where the normalization condition is given by

$$4\kappa \int_0^{\pi/2} (\sin z)^{-4/3} \psi_m(z) \psi_n(z) dz = \delta_{mn}, \quad (32)$$

to ensure the canonical four-dimensional kinetic term for $\mathcal{A}_\mu(x)$; the discrete spectrum of eigenvalues $q_n \equiv m_n$, with the corresponding eigenfunctions, can then be obtained numerically.

B. Soft-Wall models

SW models were originally motivated as holographic models with vector resonances displaying Regge trajectories. The action of SW models is given by (2), where the metric is AdS_5 , and $e^{-\Phi(z)}$ represents a nontrivial background dilaton field given by [25]

$$\Phi(z) = \kappa^2 z^2, \quad (33)$$

leading to a spectrum given by

$$m_n^2 = 4\kappa^2(n+1). \quad (34)$$

The dimensionful constant κ can be fixed by fitting the mass of the first vector resonance to that of the ρ meson, *i.e.* $\kappa = m_\rho/2$. Therefore, the equations of motion for the different fields can be obtained from those of the HW1 model by replacing the AdS_5 warp factor with $e^{-\Phi(z)}/z$. Contrary to the HW models, in the SW model the extra dimension is no longer restricted to a finite interval, *i.e.* $z_0 = \infty$ and the infrared boundary conditions are replaced by normalization conditions on wave functions and bulk-to-boundary propagators.

For the vector fields one has to solve the following equation:

$$\partial_z \left(\frac{e^{-\kappa^2 z^2}}{z} \partial_z \mathcal{J} \right) - Q^2 \frac{e^{-\kappa^2 z^2}}{z} \mathcal{J} = 0, \quad (35)$$

whose solution can be cast in the integral representation [31]

$$\mathcal{J}(Q, z) = \kappa^2 z^2 \int_0^1 \frac{x^a}{(1-x)^2} \exp \left[-\frac{x}{1-x} \kappa^2 z^2 \right] dx, \quad (36)$$

where $a = Q^2/4\kappa^2$.

One of the main drawbacks of the original SW is that chiral symmetry breaking is not implemented in a satisfactory way. Due to the absence of an infrared brane, the parameters for explicit and spontaneous symmetry breaking are not independent. This not only invalidates general relations like the GMOR, but makes the whole pion dynamics unclear. Recent proposals have tried to circumvent this problem, so far only at an heuristic level. In this paper we will adopt the prescription given in [32], where the pion wave function is assumed to be Gaussian,

$$\alpha(z) = e^{-\kappa^2 z^2}. \quad (37)$$

A comparison of the pion wave function profiles for the different models is shown in Fig. 2.

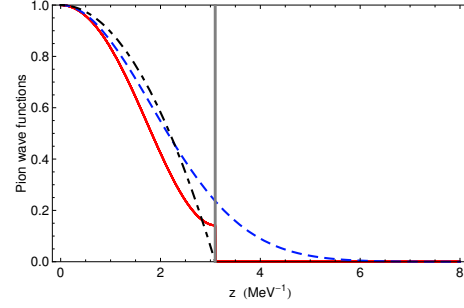


FIG. 2: Comparison of the pion wave functions of the HW1 model (red solid line), the HW2 model (black dot-dashed line) and the Gaussian ansatz of Eq. (37) (blue dashed line). The vertical line corresponds to the infrared brane at $z = z_0$.

III. $\pi^0 \gamma^* \gamma^*$ FORM FACTOR

In this Section we will apply the methods described previously for the anomalous pion form factor. We will define the $\pi^0 \gamma^* \gamma^*$ form factor as

$$\int d^4x e^{iq_1 \cdot x} \langle 0 | T \{ J_{\text{EM}}^\mu(x) J_{\text{EM}}^\nu(0) \} | \pi^0(p) \rangle \quad (38)$$

$$= \epsilon^{\mu\nu\alpha\beta} q_{1\alpha} q_{2\beta} F_{\gamma^* \gamma^* \pi^0}(Q_1^2, Q_2^2),$$

where $p = q_1 + q_2$ is the pion momentum, q_1, q_2 are the momenta of photons, and $q_{1,2}^2 = -Q_{1,2}^2$. Notice that our conventions differ by a sign from the ones used in [33, 34].

Even though the form factor cannot be computed from first principles, there are certain kinematical limits where theoretical or experimental information is available. For instance, when both photons are on-shell, the form factor is determined (in the chiral limit) solely by the WZW anomaly term

$$F_{\gamma^* \gamma^* \pi^0}(0, 0) = -\frac{N_C}{12\pi^2 f_\pi}, \quad (39)$$

and it is therefore convenient to define

$$F_{\gamma^* \gamma^* \pi^0}(Q_1^2, Q_2^2) = -\frac{N_C}{12\pi^2 f_\pi} K(Q_1^2, Q_2^2), \quad (40)$$

such that $K(0, 0) = 1$.

On the experimental side, studies have focused on the low-energy behavior, when one of the photons is exactly on-shell and the other slightly off-shell. In this kinematic regime it is common to define the slope of the anomalous form factor a_π as

$$K(0, Q^2) = K(Q^2, 0)$$

$$= \left[1 - \frac{a_\pi}{m_\pi^2} Q^2 + \frac{b_\pi}{m_\pi^4} Q^4 \dots \right], \quad (41)$$

i.e.,

$$a_\pi = -m_\pi^2 \left[\frac{dK(Q^2, 0)}{dQ^2} \right]_{Q^2=0} . \quad (42)$$

The world average is presently $a_\pi = 0.032(4)$, mainly driven by the results of the CELLO Collaboration [16] on $\pi^0 \rightarrow e^+e^-\gamma$. Given the importance of this kinematical regime for the evaluation of the $(g-2)_\mu$, we also define the curvature b_π as

$$b_\pi = m_\pi^4 \left[\frac{dK(Q^2, 0)}{dQ^4} \right]_{Q^2=0} . \quad (43)$$

Later on we will use the different holographic models to obtain a determination for both a_π and b_π .

Another source of information comes when one of the photons is on-shell and the other far off-shell. Then the expected behavior of the pion form factor is dictated by the Brodsky-Lepage quark-counting rules [35, 36],

$$\lim_{Q^2 \rightarrow \infty} K(0, Q^2) \sim \frac{1}{Q^2} . \quad (44)$$

Data on this kinematical regime is available from $e^+e^- \rightarrow e^+e^-\pi^0$. The behavior of the previous equation is reasonably reproduced by CLEO [37] but incompatible with recent data by BABAR [38]. Hopefully upcoming BABAR data with better statistics will help clarify the situation. While the discrepancy is surprising, we want to emphasize that the kinematical regime we are considering does not accept an OPE expansion and, therefore, that Eq. (44) is not on the same footing as a short-distance constraint.

Short-distance constraints can be obtained when both photons have large and equal virtualities. In this case,

$$\lim_{Q^2 \rightarrow \infty} K(Q^2, Q^2) = \frac{8\pi^2 f_\pi^2}{N_c} \frac{1}{Q^2} . \quad (45)$$

It is worth stressing that all the constraints and experimental information presented above refer to the pion being strictly on-shell. In our case, since we are working in the chiral limit, to a very good approximation $p^2 = m_\pi^2 \sim 0$. We will come back to the on-shellness of the pion when we discuss the pion exchange diagram in $(g-2)_\mu$. For the time being, we will concentrate on the pion form factor as predicted from the different holographic models.

A. Holographic predictions

In terms of holographic QCD, $K(Q_1^2, Q_2^2)$ can be obtained from the VVA terms of the Chern-Simons

action. Working in the axial gauge, $\mathcal{B}_z = 0$, and gathering the relevant pieces trilinear in the fields one finds:

$$S_{\text{CS}}^{\text{AdS}} = \frac{N_c}{24\pi^2} \epsilon^{\mu\nu\rho\sigma} \text{tr} \int d^4x dz (\partial_z \mathcal{B}_\mu) \left[\mathcal{F}_{\nu\rho} \mathcal{B}_\sigma + \mathcal{B}_\nu \mathcal{F}_{\rho\sigma} \right] . \quad (46)$$

Replacing $A_\mu = \partial_\mu \pi$ and taking the pion to be on-shell one ends up with

$$S_{\text{CS}}^{\text{AdS}} = \frac{N_c}{12\pi^2} \epsilon^{\mu\nu\rho\sigma} \int d^4x \int_0^{z_0} dz \pi^a \times \left[2 \partial_z \beta \partial_\rho V_\mu^a \partial_\sigma \hat{V}_\nu - \beta \partial_z \left(\partial_\rho V_\mu^a \partial_\sigma \hat{V}_\nu \right) \right] , \quad (47)$$

where $\beta(z)$ stands for the pion wave function, which we will denote as $\Psi(z)$ or $\alpha(z)$, depending on the model.

Integrating by parts over z in the second term above and dismissing a boundary term (cf. [33]) in order to reproduce the standard four-dimensional WZW action one gets

$$S_{\text{CS}}^{\text{AdS}} = \frac{N_c}{4\pi^2} \epsilon^{\mu\nu\rho\sigma} \int_0^{z_0} dz (\partial_z \beta) \int d^4x \pi^a (\partial_\rho V_\mu^a) (\partial_\sigma \hat{V}_\nu) . \quad (48)$$

Variation of $S_{\text{CS}}^{\text{AdS}}$ above gives the three-point function:

$$T_{\alpha\mu\nu}(p, q_1, q_2) = \frac{N_c}{12\pi^2} \frac{p_\alpha}{p^2} \epsilon_{\mu\nu\rho\sigma} q_1^\rho q_2^\sigma K(Q_1^2, Q_2^2) . \quad (49)$$

In compliance with the large- N_c limit, in extra-dimensional models the form of the interaction vertex between the pion and two external electromagnetic currents is mediated by the full tower of Kaluza-Klein vector mesons. From the variation of the Chern-Simons action with respect to the external sources one obtains

$$K(Q_1^2, Q_2^2) = - \int_0^{z_0} \mathcal{J}(Q_1, z) \mathcal{J}(Q_2, z) \partial_z \beta(z) dz + (\text{possible boundary terms}) , \quad (50)$$

where $\mathcal{J}(Q, z)$ is the vector bulk-to-boundary propagator at Euclidean momentum $Q^2 = -q^2$, defined in the previous Section.

The significance of boundary terms in the Chern-Simons action was studied in detail in [28]. In the context of the HW1 model, boundary terms in the expression of $K(Q_1^2, Q_2^2)$ were shown to be needed in order to have the right normalization required by the QCD axial anomaly, namely $K(0, 0) = 1$. The presence of these boundary terms is closely related to the infrared behavior of the pion wave function. As pointed out in Eq. (12), in the HW1 model the value of the pion wave function at z_0 does not cancel

and requires the addition of a boundary term [33]

$$K(Q_1^2, Q_2^2) = - \int_0^{z_0} \mathcal{J}(Q_1, z) \mathcal{J}(Q_2, z) \partial_z \Psi(z) dz + \mathcal{J}(Q_1, z_0) \mathcal{J}(Q_2, z_0) \Psi(z_0) . \quad (51)$$

No boundary term is needed both in the case of the HW2 and the SS models. The correct normalization is obtained in both cases (using $\mathcal{J}(0, z) = 1$) due to the boundary conditions satisfied by $\alpha(z)$:

$$K(0, 0) = - \int_0^{z_0} \partial_z \alpha(z) dz = \alpha(0) = 1 . \quad (52)$$

For the SW models, since the pion wave function is introduced by hand, it depends on the ansatz made. In general, pion wave function that do not cancel at the infrared brane will require boundary terms to correctly implement the axial anomaly in $K(Q_1, Q_2)$.

Equipped with Eqs. (50) and (51), together with the different expressions for the pion wave function and vector bulk-to-boundary propagator, one can easily find the expressions for the pion form factor. We are mostly interested in checking whether short-distance constraints are satisfied and to what extent the low-energy information complies with experimental data.

B. Large- Q^2 behavior

In asymptotically AdS holographic models, it is easy to show that the function $K(Q_1, Q_2)$ automatically satisfies the high-energy constraints discussed in the previous Section. For instance, for arbitrarily large Q_1 and Q_2 , and working in the HW2 model, it is not difficult to show that the general expression reads

$$\begin{aligned} K(w, Q^2) &\simeq \frac{2}{z_0^2 Q^2} \sqrt{1-w^2} \\ &\times \int_0^\infty d\xi K_1(\sqrt{1+w\xi}) K_1(\sqrt{1-w\xi}) \xi^3 \\ &\simeq \frac{2}{w^3 z_0^2 Q^2} [w - (1-w^2) \tanh^{-1} w] , \end{aligned} \quad (53)$$

where $w = \frac{Q_1^2 - Q_2^2}{2Q^2}$, $2Q^2 = Q_1^2 + Q_2^2$ and $\xi = Qz$.

It is easy to show that the momentum dependence of the previous result also holds for the HW1 and SW models: AdS dictates the large- Q^2 behavior of the bulk-to-boundary propagator, and this is common to all of them. Moreover, the shape of the pion wave function is very similar for all the models close to the ultraviolet boundary, as illustrated in Fig. 2.

Indeed, as pointed out in [34], $\alpha(z)$ and the pion wave function (11) coincide in the deep ultraviolet, since at small z

$$\partial_z \Psi(z) \simeq -f_\pi^2 g_5^2 z = -2 \frac{z}{z_0^2} = \partial_z \alpha(z) . \quad (54)$$

Notice that differences between HW1 and HW2 only affect the infrared of the theory, and therefore are of no relevance for the large- Q^2 behavior (at most exponentially suppressed like $\mathcal{O}(e^{-Qz_0})$).

The form of the coefficient in front of Eq. (53) will obviously change depending on the details of the model. For instance, the SW model with the *ad hoc* Gaussian pion wave function is recovered by replacing $z_0 \rightarrow 1/\kappa$. Since z_0 is related to the pion decay constant, while κ is matched to the $\rho(770)$ mass, if we impose numerical agreement between both models we find the relation

$$m_\rho^2 = 8\pi^2 f_\pi^2 , \quad (55)$$

which can be compared for instance with the prediction [39]

$$m_\rho^2 = \frac{16\sqrt{6}}{5} \pi^2 f_\pi^2 , \quad (56)$$

coming from a large- N_c sum rule analysis of Π_{VV} and Π_{AA} . It is reassuring that both predictions are in excellent agreement.

When $Q_1 = Q_2 = Q$, Eq. (53) simplifies to

$$K(Q^2, Q^2) = \frac{4}{3z_0^2 Q^2} . \quad (57)$$

With the expression for z_0 in the HW2 model, $z_0 = 2/g_5^2 f_\pi$, and $g_5^2 = 12\pi^2/N_c$, it is easy to show that it agrees with Eq. (45). Actually, one can go even further to show that the leading terms for $\lambda \rightarrow \infty$ are

$$\begin{aligned} K(\lambda^2 Q^2, (\lambda^2 Q^2 - P^2)) &\simeq \\ &\frac{2}{3} \frac{g_5^2 f_\pi^2}{Q^2} \left\{ \frac{1}{\lambda^2} + \frac{1}{\lambda^3} \frac{P \cdot Q}{Q^2} + \mathcal{O}\left(\frac{1}{\lambda^4}\right) \right\} , \end{aligned} \quad (58)$$

which, up to $\mathcal{O}(\alpha_S)$ corrections which cannot be captured by the HW2 model, is the short-distance behavior found in [4] and [40].

One can also explore the regime where one photon is on-shell and the other far off-shell. In that case,

$$K(0, Q^2) \simeq \frac{2}{z_0^2 Q^2} \int_0^\infty d\xi K_1(\xi) \xi^2 = \frac{4}{z_0^2 Q^2} = \frac{8\pi^2 f_\pi^2}{Q^2} , \quad (59)$$

which displays the Brodsky-Lepage scaling, cf. Eq. (44).

Eqs. (53), (57), (58) and (59) do not hold, however, for the models without asymptotic AdS metric, *i.e* the Sakai-Sugimoto and the flat HW2 model. At least for the latter, calculations can be performed analytically with the results

$$\begin{aligned} K(w, Q^2) &= \frac{1}{2wz_0Q} \\ &\times [\sqrt{1+w} \tanh(Qz_0\sqrt{1+w}) - \{w \rightarrow -w\}] , \\ K(Q^2, Q^2) &= \frac{1}{2Qz_0} , \\ K(0, Q^2) &= \frac{1}{Qz_0} , \end{aligned} \quad (60)$$

which fail to reproduce the OPE of QCD.

C. Small- Q^2 behavior and predictions for the parameters a_π and b_π

At small virtualities one can expand $K(Q_1^2, Q_2^2)$ in the form

$$K(Q_1^2, Q_2^2) \simeq 1 + \hat{\alpha} (Q_1^2 + Q_2^2) + \hat{\beta} Q_1^2 Q_2^2 + \hat{\gamma} (Q_1^4 + Q_2^4) . \quad (61)$$

By comparison with the previous Section, we immediately conclude that $a_\pi = -\hat{\alpha}m_\pi^2$ and $b_\pi = \hat{\gamma}m_\pi^4$. The parameter $\hat{\beta}$ does not contribute to processes when one of the photons is real. Even so, it will be a useful parameter in the determination of $(g-2)_\mu$ in Section IV.

Eq. (61) can be reproduced from holographic models by working out the small- Q^2 behavior of $\mathcal{J}(Q, z)$, which we will parametrize as

$$\mathcal{J}(Q, z) \equiv 1 - Q^2 g(z) + Q^4 h(z) . \quad (62)$$

The functions $g(z)$ and $h(z)$ can be easily obtained by solving perturbatively in Q^2 the equation of motion for the different models. This leads to the following analytic expressions:

(i) HW1 and HW2 models:

$$\begin{aligned} g(z) &= \frac{z^2}{4} \left[1 - 2 \log \left(\frac{z}{z_0} \right) \right] , \\ h(z) &= \frac{z^4}{16} \left[2 \left(\frac{z_0}{z} \right)^2 - \frac{5}{4} + \log \left(\frac{z}{z_0} \right) \right] ; \end{aligned} \quad (63)$$

(ii) SS model:

$$\begin{aligned} g(z) &= M_{KK}^{-2} \left[\int_0^z dy \frac{y}{(\sin y)^{4/3}} + z \int_z^{\pi/2} \frac{dy}{(\sin y)^{4/3}} \right] , \\ h(z) &= M_{KK}^{-2} \left[\int_0^z dy \frac{y g(y)}{(\sin y)^{4/3}} + z \int_z^{\pi/2} dy \frac{g(y)}{(\sin y)^{4/3}} \right] ; \end{aligned} \quad (64)$$

Model	$\hat{\alpha}$ (GeV $^{-2}$)	$\hat{\beta}$ (GeV $^{-4}$)	$\hat{\gamma}$ (GeV $^{-4}$)
HW1	-1.60	3.01	2.63
HW2 (AdS)	-1.81	3.65	3.06
HW2 (Flat)	-1.37	2.25	2.25
SS	-2.04	4.56	3.55
SW	-1.66	3.56	2.76

TABLE I: Values of $\hat{\alpha}$, $\hat{\beta}$ and $\hat{\gamma}$ for the holographic models discussed in the main text.

(iii) SW model:

$$\begin{aligned} g(z) &= -\frac{z^2}{4} \int_0^1 \exp \left[-\frac{x}{1-x} \kappa^2 z^2 \right] \frac{\ln x}{(1-x)^2} dx , \\ h(z) &= \frac{z^2}{32\kappa^2} \int_0^1 \exp \left[-\frac{x}{1-x} \kappa^2 z^2 \right] \frac{\ln^2 x}{(1-x)^2} dx ; \end{aligned} \quad (65)$$

(iv) flat case:

$$\begin{aligned} g(z) &= z^2 \left[\frac{z_0}{z} - \frac{1}{2} \right] , \\ h(z) &= \frac{z^4}{24} \left[1 - 4 \frac{z_0}{z} + 8 \left(\frac{z_0}{z} \right)^3 \right] . \end{aligned} \quad (66)$$

Plugging the previous expressions into Eq. (50) or (51) one can obtain the different determinations for the low-energy parameters. For the HW1 model one finds

$$\begin{aligned} \hat{\alpha} &= -\frac{z_0^2}{4} \Psi(z_0) + \int_0^{z_0} g(z) \partial_z \Psi(z) dz , \\ \hat{\beta} &= \frac{3z_0^4}{64} \Psi(z_0) - \int_0^{z_0} h(z) \partial_z \Psi(z) dz , \\ \hat{\gamma} &= \frac{z_0^4}{16} \Psi(z_0) - \int_0^{z_0} g(z)^2 \partial_z \Psi(z) dz , \end{aligned} \quad (67)$$

while for the remaining models:

$$\begin{aligned} \hat{\alpha} &= \int_0^{z_0} g(z) \partial_z \alpha(z) dz , \\ \hat{\beta} &= - \int_0^{z_0} h(z) \partial_z \alpha(z) dz , \\ \hat{\gamma} &= - \int_0^{z_0} g(z)^2 \partial_z \alpha(z) dz . \end{aligned} \quad (68)$$

The values for the different models are collected in Table I. Experimentally, only the slope has been determined, $\hat{\alpha} = -1.76(22)$ GeV $^{-2}$ [41], which is correctly reproduced by the HW1, HW2 and SW models. Notice that, even though the slope is a genuine low-energy quantity, models without an asymptotic AdS metric fail to reproduce the experimental

Model	$\hat{\alpha}_n/\hat{\alpha}$			$\hat{\beta}_n/\hat{\beta}$			$\hat{\gamma}_n/\hat{\gamma}$		
HW1	1.20	-0.18	-0.04	1.10	-0.06	0.01	1.20	-0.22	0.06
HW2 (AdS)	1.30	-0.37	0.06	1.10	-0.11	0.01	1.30	-0.37	0.08
HW2 (flat)	0.99	0.01	0.00	1.00	0.00	0.00	1.00	0.00	0.00
SS	1.70	-1.10	0.49	1.30	-0.34	0.07	1.60	-1.10	0.54
SW	0.75	0.14	0.05	0.87	0.09	0.02	0.88	0.09	0.02

TABLE II: Contribution to $\hat{\alpha}$, $\hat{\beta}$ and $\hat{\gamma}$ due to the first three vector-meson radial excitations. For $\hat{\alpha}_n$, each sub-column ($n = 1, 2, 3$) contains the contribution of $k, l \leq n$ terms. $\hat{\beta}_n$ and $\hat{\gamma}_n$ are defined analogously.

value. The quartic parameters $\hat{\beta}$ and $\hat{\gamma}$, using the phenomenologically acceptable HW1, HW2 and SW models, are predicted to be

$$\hat{\beta} = 3.33(32) \text{ GeV}^{-4}, \quad (69)$$

$$\hat{\gamma} = 2.84(21) \text{ GeV}^{-4}. \quad (70)$$

Both holographic predictions will be used in the evaluation of the HLBL contribution to the $(g-2)_\mu$.

D. A comment on lowest meson dominance

Before moving to the evaluation of the $(g-2)_\mu$, it is important to explore the resonance contributions to the results of Table 1. For this, we write the vector bulk-to-boundary propagator in its spectral decomposition

$$\mathcal{J}(z, Q) = \sum_{n=1}^{\infty} \frac{f_n}{Q^2 + m_n^2} \psi_n(z), \quad (71)$$

where m_n is the mass of the n th vector resonance and f_n is related to its decay constant. Plugging this expression into Eq. (50), one obtains the double series

$$K(Q_1^2, Q_2^2) \equiv \sum_{k,l=1}^{\infty} \frac{B_{kl}}{(Q_1^2 + m_k^2)(Q_2^2 + m_l^2)}. \quad (72)$$

This expression is of the form expected in the large- N_c limit, with the full tower of vector mesons propagating between the pion and the two photons. The contributions for $\hat{\alpha}$, $\hat{\beta}$ and $\hat{\gamma}$ from the first three vector radial excitations are reported in Table II. The important point to notice is that lowest vector dominance is a feature common to all models (from the practically ρ -dominance of the flat model to the more moderate behavior of the SS model). Incidentally, notice also that, with the exception of the SW model, the contribution of the first resonance tends to overshoot the total value and has to be compensated by negative contributions from higher-order

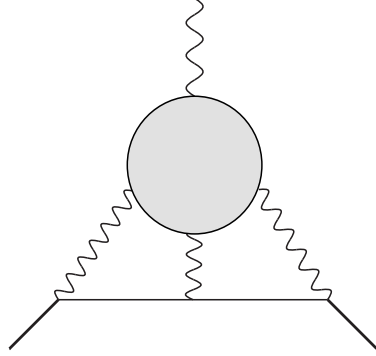


FIG. 3: Hadronic light by light contribution to $(g-2)_\mu$.

resonances. Finally, let us remark that the representation of Eq. (72) is only reliable for moderate values of the resonance indices. Most likely Eq. (72) is, at most, an asymptotic expansion and, therefore, beyond a certain threshold it ceases to be meaningful.

IV. THE HADRONIC LIGHT BY LIGHT CONTRIBUTION TO THE $(g-2)_\mu$

With experimental accuracies at the 10^{-10} level, precise determinations of the HLBL contribution to the $(g-2)_\mu$ become of paramount importance. The problem is that genuine nonperturbative techniques are required and having theoretical uncertainties under control is certainly a challenging task. The HLBL contribution to the $(g-2)_\mu$ is depicted in Fig. 3. When internal momenta in the loop are high enough one can use perturbation theory, but a proper evaluation also requires low energies, *i.e.* Goldstone bosons and hadrons. The neutral pion exchange contribution, depicted in Fig 4, turns out to be the dominant piece ($a_\mu^{(\pi^0)} \sim 7 \cdot 10^{-10}$) followed by the η and η' contributions ($a_\mu^{(\eta, \eta')} \sim 3 \cdot 10^{-10}$). Quark and Goldstone loops, axial-vectors and scalars are also expected to contribute at the level of $(1-2) \cdot 10^{-10}$, but cancellations occur (scalars and Goldstone loops contribute negatively) and so the Goldstone boson exchange ends up collecting the bulk of the effect. In particular, this means that the naive large- N_c counting works and single-resonance exchange is the dominant effect. This observation suggests that procedures based on the $1/N_c$ framework are suitable tools to address the problem.

Different parametrizations have been used in the past to evaluate the HLBL contribution. In particular, there is the detailed study of [4] with different parametrizations based on LMD. Having in mind what we did so far, one could be tempted to

use the results of the previous Section on the pion form factor to evaluate each of the $\pi^0\gamma\gamma$ vertices in Fig. 4, as has been recently done for the HW1 model [42]. However, in this paper we want to be able to test the pion-pole approximation. In order to do so, one should trade the $\pi^0\gamma\gamma$ form factor for the more general objects $P^0\gamma\gamma$ or $A^0\gamma\gamma$. The issue of on-shellness versus off-shellness of the pion has attracted some attention in recent years [6, 43, 44]. Here we will follow the approach taken in [6] and characterize the degree of off-shellness entirely by the short-distance constraint

$$\lim_{Q^2 \rightarrow \infty} F_{\pi^0\gamma^*\gamma^*}(Q^2, Q^2, 0) = -\frac{f_\pi}{3}\chi_0 + \dots \quad (73)$$

From the previous expression one readily sees that the degree of off-shellness is then regulated by the parameter χ_0 . Unfortunately, this parameter is only poorly known. We will discuss this issue and its impact on the $(g-2)_\mu$ at the end of this Section.

Our strategy to test the pion-pole approximation will be the following:

- (i) We will use the following ansatz for the form factor:

$$K(q_1^2, q_2^2) = 1 + \lambda \left(\frac{q_1^2}{q_1^2 - m_V^2} + \frac{q_2^2}{q_2^2 - m_V^2} \right) + \eta \frac{q_1^2 q_2^2}{(q_1^2 - m_V^2)(q_2^2 - m_V^2)}, \quad (74)$$

first introduced in the context of $K_L \rightarrow \mu^+ \mu^-$ decays [18]. This parametrization was originally put forward to study the low-energy slope of three-point functions, and has been used in experimental studies of $K_L \rightarrow \mu^+ \mu^-$ and $K_L \rightarrow \pi^0 e^+ e^-$.

- (ii) We will promote the ansatz in (74) to an analytic interpolator valid for any value of the photon momenta. Then, using Eqs. (40) and (73), we get an expression for χ_0 in terms of the linear slope λ

$$\chi_0 = \frac{N_c}{4\pi^2 f_\pi^2} (1 + \lambda). \quad (75)$$

Aside from being simple and with a very intuitive low-energy behavior, the parametrization of Eq. (74) has additional advantages. One of the most important is that the computation of $(g-2)_\mu$ turns out to be greatly simplified. In Ref. [4] it was shown that if the interpolator can be cast in the generic form:

$$F_{\pi^0\gamma^*\gamma^*}(q_1^2, q_2^2) = -\frac{N_c}{12\pi^2 f_\pi} \left[f(q_1^2) - \sum_i \frac{1}{q_2^2 - m_i^2} g_i(q_1^2) \right], \quad (76)$$

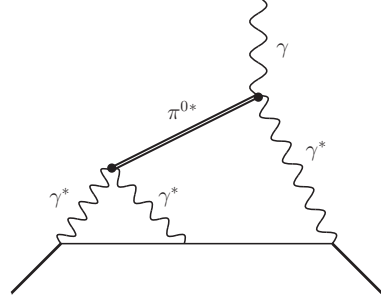


FIG. 4: One of the diagrams contributing to pion exchange in the HLBL contribution to $(g-2)_\mu$.

then, in the general two-loop expression for the pion contribution to the HLBL scattering, all angular integrations can be performed using the hyperspherical approach. The diagram of Fig. 4 can then be evaluated through the following expression:

$$a_\mu^{\pi^0} = \left(\frac{\alpha_{em}}{\pi} \right)^3 \left\{ a_{\mu(1)}^{\pi^0} + a_{\mu(2)}^{\pi^0} \right\}, \quad (77)$$

where

$$a_{\mu(1)}^{\pi^0} = \int_0^\infty dQ_1 \int_0^\infty dQ_2 \left[w_1(Q_1, Q_2) G_1(Q_1, Q_2) + w_2(m_V, Q_1, Q_2) G_2(Q_1, Q_2) \right] \quad (78)$$

and

$$a_{\mu(2)}^{\pi^0} = \int_0^\infty dQ_1 \int_0^\infty dQ_2 \left[w_3(m_V, Q_1, Q_2) G_3(Q_1, Q_2) + w_3(m_\pi, Q_1, Q_2) G_4(Q_1, Q_2) \right]. \quad (79)$$

In the previous expressions, G_i are generalized form factors and w_i weight factors, whose expressions are given in Appendix A.

In other words, the contribution to the $(g-2)_\mu$ can be reduced to a more tractable double integral. It is not difficult to verify that the interpolator of Eq. (74) is of the form (76) with

$$f(q^2) = 1 + \lambda + (\lambda + \eta) \frac{q^2}{q^2 - m_V^2}, \quad (80)$$

$$g_V(q^2) = -m_V^2 \left[\lambda + \eta \frac{q^2}{q^2 - m_V^2} \right]. \quad (81)$$

Notice that the interpolator of Eq. (74) is assumed not to depend on the pion momentum. This simplifying assumption, together with the specific form of Eq. (76), is crucial to be able to use Eqs. (78) and (79).

Our parametrization has 3 free parameters, λ , η and m_V which will be determined by combining the

following constraints:

$$\frac{\lambda}{m_V^2} = (-1.76 \pm 0.22) \text{ GeV}^{-2}, \quad (82)$$

$$1 + 2\lambda + \eta = 0, \quad (83)$$

$$\lambda + \eta = -\frac{4\pi^2 f_\pi^2}{3m_V^2}. \quad (84)$$

The first one is a low-energy experimental constraint on the slope of the pion form factor (the $\hat{\alpha}$ parameter of the previous Section), while the last two are short-distance information, namely the requirement that $K(Q^2, Q^2)$ at high energies does not go like a constant (first equation) and that its $1/Q^2$ behavior has the right coefficient (see Eq. (45), with $N_c = 3$).

Using as input parameters

$$\begin{aligned} m_\mu &= 105.658367(4) \text{ MeV}, \\ m_\pi &= 134.9766(6) \text{ MeV}, \\ f_\pi &= 92.4 \text{ MeV}, \\ \alpha_{em} &= 1/137.03599976, \end{aligned} \quad (85)$$

the parameters of the model become

$$\begin{aligned} \lambda &= -0.73 \pm 0.05, \\ \eta &= 0.46_{-0.13}^{+0.10}, \\ m_V &= (0.64_{-0.06}^{+0.07}) \text{ GeV}, \\ \chi_0 &= (2.42 \pm 0.17) \text{ GeV}^{-2}, \end{aligned} \quad (86)$$

where the uncertainties are due to the experimental error on the slope.

Several comments are relevant at this point:

- (i) The values of $\hat{\beta}$ from the HW1 and HW2 models in Table I are in very good agreement with the value of η ($\sim \hat{\beta}m_V^4$) in Eqs. (86). We have already mentioned that also the linear slope, λ , is very well reproduced by HW1 and HW2 in Table I.
- (ii) The value we find for the mass scale has to be interpreted as an effective measure of the relevant scale for the problem. Therefore, we confirm that m_ρ is indeed very close to the natural scale to estimate the pion exchange contribution.
- (iii) The prediction for χ_0 in (86) is obtained from the requirement that DIP is a good interpolator also for an off-shell pion and uses only the phenomenological linear slope, λ (and not the holographic one). However, the result would have been very similar by trading the phenomenological linear slope with the holographic values predicted by HW1 and HW2.

- (iv) In order to test the stability and improve the accuracy of the results on HLBL one can add an extra pole to the interpolator. We shall follow this line of thought later on.

With the values given in Eq. (86), the prediction for the anomalous magnetic moment is

$$a_\mu^{\pi^0} = 6.7(3) \cdot 10^{-10}. \quad (87)$$

In Table III the comparison is made with the LMD result quoted in Ref. [4]. In LMD models it is common to identify $m_V \equiv m_\rho$. In contrast, in our case the mass scale is determined dynamically by the constraints. The first thing to realize is that the contributions for each integral (each column in Table III) are in good agreement, even though the interpolators are very different and $m_V = 0.64 \text{ GeV} \neq m_\rho$. However, if we redo our analysis but now set $m_V = m_\rho$ from the start (and ignore Eq. (82)), then there is *full* agreement with LMD (third line of Table III). Thus, the previous exercise implies that the difference between LMD and our approach is entirely due to the choice of mass scale, which in our case is determined self-consistently. Therefore, while lowest meson dominance might be a reasonable strategy when little information about the correlator is known, with the present status of the HLBL, it seems more justified to take full advantage of the available information.

A. Extension of the DIP ansatz

The interpolator considered in the previous Section provided an estimate for the HLBL that fulfilled the leading long and short-distance constraints from $F_{\pi^0\gamma^*\gamma^*}$. However, as we stated in the introduction, in this paper we want to investigate the dependence on the low-energy parameters $\hat{\beta}$ and $\hat{\gamma}$ and estimate the impact of the pion away from its mass shell.

The parameters $\hat{\beta}$ and $\hat{\gamma}$ were computed in Section III, Eqs.(69) and (70). In order to understand their potential importance for the HLBL, in Fig. 5 we show the shape of the weight functions entering the dominant $a_{\mu(1)}^{\pi^0}$. As pointed out in [4], the relevant contributions are highly peaked at low values of momenta, $0 \leq Q^2 \lesssim 0.5 \text{ GeV}$. Therefore, this suggests that more information on (very) low energies can help improve the determination of a_μ .

In order to check the stability of the results obtained so far, in particular Eqs. (86), we consider a generalization of the DIP interpolator by adding an

Model	$w_1 G_1$	$w_2 G_2$	$w_3 G_3$	$w_4 G_4$	a_μ
LMD	+0.015	+0.042	+0.0016	-0.0002	$7.3 \cdot 10^{-10}$
DIP $_{\hat{\alpha}}$	+0.018(3)	+0.034(4)	+0.0016	-0.0002	$6.7(3) \cdot 10^{-10}$
DIP $_{m_\rho}$	+0.015	+0.043	+0.0016	-0.0002	$7.35 \cdot 10^{-10}$

TABLE III: Determination of a_μ with the DIP parametrization: in the second row, the mass scale is determined dynamically while, in the third row, $m_V = m_\rho$. Comparison is made with the LMD model. We explicitly show the contribution from the different generalized form factors G_i .

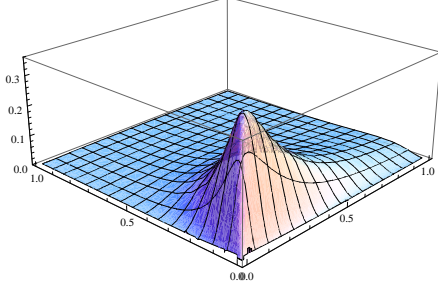


FIG. 5: The integrand of Eq. (78).

extra pole:

$$K(q_1, q_2) = 1 + \sum_i^2 \lambda_i \left(\frac{q_1^2}{q_1^2 - m_i^2} + \frac{q_2^2}{q_2^2 - m_i^2} \right) + \sum_i^2 \eta_i \frac{q_1^2 q_2^2}{(q_1^2 - m_i^2)(q_2^2 - m_i^2)}. \quad (88)$$

Notice that this increase in the number of poles, which is also natural from a large- N_c perspective, makes Eq. (88) still compatible with the general form of Eq. (76), now with

$$f(q^2) = 1 + \sum_i^2 \lambda_i + \sum_i^2 (\lambda_i + \eta_i) \frac{q^2}{q^2 - m_i^2}, \quad (89)$$

$$g_i(q^2) = -m_i^2 \left[\lambda_i + \eta_i \frac{q^2}{q^2 - m_i^2} \right]. \quad (90)$$

Therefore, the HLBL contribution can still be computed with the double integrals of Eqs. (78) and (79). By expanding Eq. (88) at low and high energies and matching it afterwards to the information coming from QCD short distances and low-energy (experimental and holographic) input, the constraints we would like to impose take the following form:

(a) Long-distance constraints:

$$\sum_i^2 \frac{\lambda_i}{m_i^2} = (-1.76 \pm 0.22) \text{ GeV}^{-2}, \quad (\text{exp.}) \quad (91)$$

$$\sum_i^2 \frac{\eta_i}{m_i^4} = (3.33 \pm 0.32) \text{ GeV}^{-4}, \quad (\text{pred.}) \quad (92)$$

$$\sum_i^2 \frac{\lambda_i}{m_i^4} = (-2.84 \pm 0.21) \text{ GeV}^{-4}, \quad (\text{pred.}) \quad (93)$$

which correspond to the low-energy parameters $\hat{\alpha}$, $\hat{\beta}$ and $\hat{\gamma}$ defined in the previous Section. The value for $\hat{\alpha}$ is taken from experiment, while $\hat{\beta}$ and $\hat{\gamma}$ are estimated from the spread of values predicted by the HW1, HW2 and SW models and given in Eqs. (69) and (70).

(b) Short-distance constraints:

$$1 + 2 \sum_i^2 \lambda_i + \sum_i^2 \eta_i = 0, \quad (94)$$

$$\sum_i^2 m_i^2 (\lambda_i + \eta_i) = -\frac{4\pi^2 f_\pi^2}{3}, \quad (95)$$

$$1 + \sum_i^2 \lambda_i = \frac{4\pi^2 f_\pi^2}{3} \chi_0. \quad (96)$$

The first two are the ones already discussed in the previous Sections, namely the absence of constant terms and the matching of the $1/Q^2$ coefficient. The last condition comes from Eq. (73).

We have already mentioned that the DIP interpolator (and its extensions) do not depend, by construction, on the pion momentum. While this allows us to use Eqs. (78) and (79), we want to note at this point that this simplifying assumption implies that Eq. (96) above and the Brodsky-Lepage constraint cannot be satisfied simultaneously (unless $\chi_0 = 0$). However, there are reasons to expect that the Brodsky-Lepage constraint plays a minor role in HLBL. First and foremost, the kernel entering $(g-2)_\mu$ is peaked at low energies (see Fig. 5) and presumably information on the high-energy region will have a negligible impact on the anomalous magnetic

moment. In this respect, it is quite reassuring that our analysis, in which the $F_{\pi^0\gamma^*\gamma^*}$ low-energy region is approximately captured by Eqs. (91)-(93), turns out to be in very good agreement with analyses that comply with the Brodsky-Lepage constraint [4, 6].

The detailed solution of the system of Eqs. (91)-(96) is given in Appendix B. The main conclusion of the analyses is that there is a remarkable stability when either $\hat{\beta}$ or $\hat{\gamma}$ are added as input. Furthermore, the uncertainty on $(g-2)_\mu$ is dominated by $\hat{\alpha}$, while the effect from $\hat{\beta}$ and $\hat{\gamma}$ is subleading. Our estimate for the pion contribution to the HLBL is

$$a_\mu = 6.54(25) \cdot 10^{-10}. \quad (97)$$

B. Impact of χ_0 on $(g-2)_\mu$

Since χ_0 cannot be accessed experimentally, one has to resort to nonperturbative techniques to estimate it. However, the different available estimates show strong discrepancies: while recent results based on QCD sum rules [45] or exclusive B decays [46] seem to favor values hovering around $\chi_0 \sim 2 - 4 \text{ GeV}^{-2}$, estimates based on the axial anomaly [47, 48], Pade approximants [49] or the original sum rule determination of [50] point at much higher values, $\chi_0 \sim 8 - 11 \text{ GeV}^{-2}$. A recent result in the context of holographic QCD [51] also pointed out the possibility that $\chi_0 \sim 0$. Most of these estimates are given without reference to the renormalization scale. However, its low-energy scale evolution was studied in [52] and does not account for the discrepancies found. Therefore, the best one can do at present is to consider a conservative $0 \leq \chi_0 \leq 8.9 \text{ GeV}^{-2}$.

The result in Eq. (97) is obtained assuming that $\chi_0 \sim (1 - 3) \text{ GeV}^{-2}$, which seems to be the range of values favored by our interpolator (see Table V in Appendix B). However, larger values of $\chi_0 \sim 9 \text{ GeV}^{-2}$, which at present cannot be excluded, might induce a shift of at most 15%. Given the precision presently needed for the $(g-2)_\mu$, we believe that a better understanding of χ_0 is essential.

V. CONCLUSIONS

The muon anomalous magnetic moment is one of the most precisely measured quantities in particle physics, and thus a key parameter to test the appearance of physics beyond the Standard Model. With experimental accuracies expected to soon reach the 10^{-10} level, it is essential to have the theoretical uncertainties in the hadronic light-by-light scattering contribution well under control.

In this paper we have studied the electromagnetic pion form factor $F_{\pi^0\gamma\gamma}$ with a set of holographic models. We have shown that only a restricted set of the holographic models studied in Section II, *i.e.* HW1, HW2 and a modified version of SW, are able to predict a value of the linear slope compatible with the experimental data. Within this restricted set of models we have then obtained, in Section III, predictions for the quadratic slopes

$$\begin{aligned} \hat{\beta} &= 3.33(32) \text{ GeV}^{-4}, \\ \hat{\gamma} &= 2.84(21) \text{ GeV}^{-4}. \end{aligned} \quad (98)$$

Notice that, because of the holographic models used, the previous predictions are sensitive to the way chiral symmetry breaking is implemented and whether the spectrum is Regge-like or not (SW versus HW). This sensitivity is contained in the quoted uncertainty.

We have then introduced an interpolator for the form factor that encodes both short distances (coming from QCD) and long distances (the quadratic slopes $\hat{\beta}$ and $\hat{\gamma}$ predicted above together with the experimental linear slope $\hat{\alpha}$) and computed the pion exchange HLBL contribution to the $(g-2)_\mu$. Following [6], we have also estimated the effects due to a departure from the pion-pole approximation through a new short-distance constraint for $F_{\pi^0\gamma^*\gamma^*}$, which is controlled by the parameter χ_0 . Our final number for the (pion exchange) HLBL contribution is

$$a_\mu^{\pi^0} = (6.54 \pm 0.25) \cdot 10^{-10}, \quad (99)$$

which depends on the slope ($\hat{\alpha}$) and curvature ($\hat{\beta}$ and $\hat{\gamma}$) of $F_{\pi^0\gamma^*\gamma^*}$ as well as on the parameter χ_0 . Our analysis shows that, while $\hat{\beta}$ and $\hat{\gamma}$ are important ingredients, the uncertainty is currently dominated by the experimental accuracy on $\hat{\alpha}$. In view of this, improvements on the slope $\hat{\alpha}$ should be a priority. Actually, this is one of the main points in the scientific program for the KLOE-2 proposal [11] at DAΦNE in Frascati. With high enough statistics, it is even feasible that the holographic predictions for $\hat{\beta}$ and $\hat{\gamma}$ could be tested.

Another sizable source of uncertainty comes from the parameter χ_0 . Our result in Eq. (99) assumes $0 \lesssim \chi_0 \lesssim 3 \text{ GeV}^{-2}$. While numbers hovering around $\chi_0 \sim 2 \text{ GeV}^{-2}$ seem to be favored by our analysis and also by different theoretical estimations, higher values ($\chi_0 \sim 9 \text{ GeV}^{-2}$) have also been reported in the literature. These higher values for χ_0 would induce a (10 – 15)% shift on the HLBL contribution. Therefore, we want to emphasize the need to put stronger bounds on the current value of χ_0 . In particular, a lattice determination of χ_0 would be extremely useful.

Finally, the effects of model dependence in our approach are evaluated in two ways: first, through the spread of values for the low-energy quartic terms in $F_{\pi^0\gamma^*\gamma^*}$, coming from the different holographic models; and second, using different versions for the parametrization of $F_{\pi^0\gamma^*\gamma^*}$. The resulting uncertainties are negligible, as it can be seen in Table IV.

We have also compared our analysis with LMD models. In Section III we have investigated the issue of LMD in $F_{\pi^0\gamma^*\gamma^*}$ with holographic models, which contain a full spectrum of resonances. Our conclusion is that LMD is a sound approximation. This is confirmed later on in our evaluation of the HLBL: the mass scale of our interpolator, which is determined dynamically, is always close to m_ρ . In other words, the LMD observed in $(g-2)_\mu$ is a consequence of LMD in the $F_{\pi^0\gamma^*\gamma^*}$, a feature that holographic realizations successfully predict. A natural consequence of LMD is that the curvature $\hat{\gamma}$ of the pion form factor can be estimated in terms of the slope $\hat{\alpha}$

$$\hat{\gamma} = -\frac{\hat{\alpha}}{m_V^2} \sim 2.97 \text{ GeV}^{-4}, \quad (100)$$

which agrees well with the holographic prediction. Also $\hat{\beta}$ can be estimated from LMD, but an additional ingredient has to be provided. If one uses the first *short-distance* constraint coming from the DIP interpolator and combines it with lowest vector dominance setting $m_V \sim m_\rho$, one finds

$$\hat{\beta} = -\frac{2m_V^2\hat{\alpha} + 1}{m_V^4} \sim 3.10 \text{ GeV}^{-4}, \quad (101)$$

again in remarkable agreement with the holographic prediction. This also means that the *short-distance* constraint in the DIP interpolators is satisfied to a very good approximation by the low-energy values predicted by holographic models. This compatibility between long and short distances is of considerable importance. Since the previous results are mostly based on ρ -dominance in conjunction with our DIP interpolator, we conjecture that they might have a broader applicability, not just in $\pi^0 \rightarrow \gamma\gamma$ but also in leptonic and semileptonic decays, *e.g.*, $K_L \rightarrow \mu^+\mu^-$ and $K_L \rightarrow \pi^0 e^+ e^-$. In particular, it opens up a way to estimate $\hat{\beta}$ in $K_L \rightarrow (\mu^+\mu^-, \pi^0 e^+ e^-)$.

However, when it comes to the evaluation of the HLBL, within the current precision LMD is probably not good enough. We have shown that the discrepancy between our result and the one from LMD models originates entirely from the different choices of the effective mass scale: while LMD assumes $m_V = m_\rho$, in our approach the mass is determined from the matching conditions. Since this deviation is comparable to the typical uncertainty on HLBL, assuming $m_V = m_\rho$ does not seem justified.

Acknowledgments

We want to thank A. Nyffeler for correspondence and useful comments on the first version of this manuscript. O. C. wants to thank the University of Naples for very pleasant stays during the different stages of this work. L. C. and G. D'A. are supported in part by the EU under Contract No. MTRN-CT-2006-035482 (FLAVIANet), by MIUR, Italy, under Project No. 2005-023102 and by Fondo dipartimentale per la ricerca 2009. O. C. is supported by the EU under Contract No. MTRN-CT-2006-035482 (FLAVIANet) and by MICINN, Spain under Grants No. FPA2007-60323 and Consolider-Ingenio 2010 CSD2007-00042 CPAN.

Appendix A

The generalized form factors G_i entering Eqs. (78,79) are given by

$$\begin{aligned} G_1(x, y) &= -\frac{N_c}{12\pi^2 f_\pi} f(-x^2) F_{\pi^0\gamma^*\gamma^*}(-y^2, 0), \\ G_2(x, y) &= -\frac{N_c}{12\pi^2 f_\pi} \frac{g(-x^2)}{m_V^2} F_{\pi^0\gamma^*\gamma^*}(-y^2, 0), \\ G_3(x, y) &= -\frac{N_c}{12\pi^2 f_\pi} \frac{g(0)}{m_\pi^2 - m_V^2} F_{\pi^0\gamma^*\gamma^*}(-x^2, -y^2), \\ G_4(x, y) &= -\frac{N_c}{12\pi^2 f_\pi} f(0) F_{\pi^0\gamma^*\gamma^*}(-x^2, -y^2) - G_3(x, y), \end{aligned} \quad (A1)$$

while the weight factors w_i take the form

$$\begin{aligned}
w_1(x, y) = & \frac{\pi^2}{6m_\mu^2 xy(y^2 + m_\pi^2)} [4(y^2 - 2m_\mu^2)(x^2 - y^2)^2 \log(1 + \lambda(0, x, y)) \\
& + ((x^6 + y^6) - x^2 y^4 - 3x^4 y^2 + \frac{x^4 y^6}{2m_\mu^4} - \frac{x^4 y^4}{m_\mu^2} - 4m_\mu^2 x^2 y^2 - (x^2 - y^2)^2 \eta_0) \left(1 - \frac{\xi(x)}{x^2}\right) \\
& + y^2(y^4 - 4m_\mu^4) \frac{\xi(x)}{m_\mu^2} - x^4(y^2 - 2m_\mu^2)^2 \frac{\xi(y)}{2m_\mu^4} + (y^2 - 2m_\mu^2)(x^2 y^2 - 2m_\mu^2(x^2 + y^2)) \frac{\xi(x)\xi(y)}{2m_\mu^4}] , \quad (\text{A2})
\end{aligned}$$

$$\begin{aligned}
w_2(m, x, y) = & \frac{\pi^2}{6m_\mu^2 xy(y^2 + m_\pi^2)} [4(y^2 - 2m_\mu^2)(x^2 - y^2)^2 \log(1 + \lambda(0, x, y)) \\
& - 4(y^2 - 2m_\mu^2)(m^4 + (x^2 - y^2)^2 + 2m^2(x^2 + y^2)) \log(1 + \lambda(m, x, y)) \\
& + \left\{ (m^4 + 2m^2(x^2 + y^2) + (x^4 + y^4) - 2x^2 y^2) \eta_m - \frac{m^2}{m_\mu^2} x^2 (y^2 - 2m_\mu^2) \xi(y) + \frac{m^2}{m_\mu^2} x^2 y^4 \right. \\
& \left. - (x^2 - y^2)^2 \eta_0 - m^6 - 3m^4(x^2 + y^2) - 3m^2(x^4 + y^4) - 2m^2 x^2 y^2 \right\} \left(1 - \frac{\xi(x)}{x^2}\right) \Big] , \quad (\text{A3})
\end{aligned}$$

$$\begin{aligned}
w_3(m, x, y) = & \frac{\pi^2}{6m_\mu^2 xy} [4(x^2 - y^2)(m_\mu^2(y^2 - x^2) + 2x^2 y^2) \log(1 + \lambda(0, x, y)) + 4 \log(1 + \lambda(m, x, y)) \\
& \times (m^4 m_\mu^2 + (x^2 - y^2)(m_\mu^2(x^2 - y^2) - 2x^2 y^2) + 2m^2(m_\mu^2(x^2 + y^2) + x^2 y^2)) + m^4(x^2 + y^2) \\
& + 2m^2(x^4 + y^4) - m^2 x^2 y^2 - m^2(m^2 + 2x^2 + y^2) \xi(x) - m^2(m^2 - 3x^2 + 2y^2) \xi(y) - m^2 \xi(x) \xi(y) \\
& + \{(x^2 + y^2) \eta_0 - (m^2 + x^2 + y^2) \eta_m\} (x^2 - \xi(x)) + \{(y^2 - 3x^2) \eta_0 - (m^2 + y^2 - 3x^2) \eta_m\} (y^2 - \xi(y))] . \quad (\text{A4})
\end{aligned}$$

In the previous expressions we have defined

$$\lambda(m, x, y) = \frac{(m^2 + x^2 + y^2 - \eta_m)(x^2 - \xi(x))(y^2 - \xi(y))}{8m_\mu^2 x^2 y^2} , \quad (\text{A5})$$

$$\eta_m = \sqrt{(m^2 + x^2 + y^2)^2 - 4x^2 y^2} , \quad (\text{A6})$$

and

$$\xi(z) = \sqrt{z^4 + 4m_\mu^2 z^2} . \quad (\text{A7})$$

Appendix B

We start from the generalized interpolator:

$$\begin{aligned}
K(q_1, q_2) = & 1 + \sum_i \lambda_i \left(\frac{q_1^2}{q_1^2 - m_i^2} + \frac{q_2^2}{q_2^2 - m_i^2} \right) \\
& + \sum_i \eta_i \frac{q_1^2 q_2^2}{(q_1^2 - m_i^2)(q_2^2 - m_i^2)} , \quad (\text{B1})
\end{aligned}$$

whose expansion at low and high energies leads to the system of constraints of Eqs. (91)-(96). Our purpose is to investigate the impact of the low-energy

parameters $\hat{\beta}$, $\hat{\gamma}$ and χ_0 . This we will do by varying the combination of constraints to be imposed on Eq. (B1).

First let us concentrate on the parameters $\hat{\beta}$. The system of equations we have to solve is then

$$\begin{aligned}
\sum_i^2 \frac{\lambda_i}{m_i^2} &= -1.76(22) \text{ GeV}^{-2} , \quad (\text{exp.}) \\
\sum_i^2 \frac{\eta_i}{m_i^4} &= 3.33(32) \text{ GeV}^{-4} , \quad (\text{pred.}) \\
1 + 2 \sum_i^2 \lambda_i + \sum_i^2 \eta_i &= 0 , \\
\sum_i^2 m_i^2 (\lambda_i + \eta_i) &= -\frac{4\pi^2 f_\pi^2}{3} . \quad (\text{B2})
\end{aligned}$$

In order to ensure a solution, we will set $m_2 = m_\rho = 0.775 \text{ GeV}$ and $\lambda_2 = 0$. The interpolator, therefore,

reduces to

$$K_{(1)}(q_1, q_2) = 1 + \lambda \left(\frac{q_1^2}{q_1^2 - m_1^2} + \frac{q_2^2}{q_2^2 - m_1^2} \right) + \sum_i^2 \eta_i \frac{q_1^2 q_2^2}{(q_1^2 - m_i^2)(q_2^2 - m_i^2)} . \quad (\text{B3})$$

In order to check for stability, we will also consider the setting in which $m_2 = m_\rho = 0.775$ GeV and $\eta_2 = 0$. The corresponding interpolator then reads

$$K_{(2)}(q_1, q_2) = 1 + \sum_i^2 \lambda_i \left(\frac{q_1^2}{q_1^2 - m_i^2} + \frac{q_2^2}{q_2^2 - m_i^2} \right) + \eta \frac{q_1^2 q_2^2}{(q_1^2 - m_1^2)(q_2^2 - m_1^2)} . \quad (\text{B4})$$

The advantage of dealing with two generalized expressions is that we will be able to assess the dependence of our results on the specific form of the interpolator. We will denote the previous setting as $\text{DIP}_{\hat{\beta}; m_2=m_\rho}^{(i)}$, where the superscript refers to the different interpolator used ($K_{(1)}$ or $K_{(2)}$) and the subscript emphasizes that m_2 has been fixed and that $\hat{\beta}$ has been used as input. The results for the HLBL are shown in the second and third rows of Table IV and can be compared with the result from $\text{DIP}_{\hat{\alpha}}$, which corresponds to the single resonance analysis (see Table III) in the main text. The stability of the results is remarkable, as can be seen from the fact that the dependence on the parametrization ($K_{(1)}$ or $K_{(2)}$) turns out to be very mild.

An analogous analysis can be done for $\hat{\gamma}$. The only difference is that now the system of matching equations looks like

$$\begin{aligned} \sum_i^2 \frac{\lambda_i}{m_i^2} &= -1.76(22) \text{ GeV}^{-2} , \text{ (exp.)} \\ \sum_i^2 \frac{\lambda_i}{m_i^4} &= -2.84(21) \text{ GeV}^{-4} , \text{ (pred.)} \\ 1 + 2 \sum_i^2 \lambda_i + \sum_i^2 \eta_i &= 0 , \\ \sum_i^2 m_i^2 (\lambda_i + \eta_i) &= -\frac{4\pi^2 f_\pi^2}{3} . \end{aligned} \quad (\text{B5})$$

The entries in Table IV are $\text{DIP}_{\hat{\gamma}; m_2=m_\rho}^{(i)}$. From the results, we see again that the different determinations agree within errors, but somehow the uncertainty associated with $\hat{\alpha}$ has grown.

A conservative estimate, taking into account the first five rows of Table IV would give

$$a_\mu = 6.4(5) \cdot 10^{-10} . \quad (\text{B6})$$

The main source of uncertainty comes from the slope $\hat{\alpha}$, while the effect of $\hat{\beta}$ or $\hat{\gamma}$ is subleading. Thus, an improvement of the CELLO data on the slope of the $\pi^0 \gamma \gamma$ form factor can help decrease the theoretical uncertainty on the HLBL.

The previous estimate for a_μ most probably overestimates the uncertainty. Notice that the results for $\text{DIP}_{\hat{\gamma}}^{(1,2)}$ give lower values of a_μ (due to a strong suppression of $w_1 G_1$) and with bigger uncertainties from $\hat{\alpha}$. This might be a consequence of the strong correlation between $\hat{\alpha}$ and $\hat{\gamma}$ in the interpolator we are using and, therefore, such an uncertainty might be misleading. Relying on $\text{DIP}_{\hat{\beta}}^{(1,2)}$ and $\text{DIP}_{\hat{\alpha}}$ only, a more realistic estimate is

$$a_\mu = 6.54(25) \cdot 10^{-10} . \quad (\text{B7})$$

Next we turn to the evaluation of the impact of χ_0 . For this we will keep $K_{(1)}$ and $K_{(2)}$ but, instead of setting $m_2 = m_\rho$, we will add the short-distance constraint involving χ_0 to Eq. (B2):

$$\begin{aligned} \sum_i^2 \frac{\lambda_i}{m_i^2} &= -1.76(22) \text{ GeV}^{-2} , \text{ (exp.)} \\ \sum_i^2 \frac{\eta_i}{m_i^4} &= 3.33(32) \text{ GeV}^{-4} , \text{ (pred.)} \\ 1 + 2 \sum_i^2 \lambda_i + \sum_i^2 \eta_i &= 0 , \\ \sum_i^2 m_i^2 (\lambda_i + \eta_i) &= -\frac{4\pi^2 f_\pi^2}{3} , \\ 1 + \sum_i^2 \lambda_i &= \frac{4\pi^2 f_\pi^2}{3} \chi_0 . \end{aligned} \quad (\text{B8})$$

We will denote the resulting interpolators as $\text{DIP}_{\hat{\beta}; \chi_0}^{(i)}$. Accordingly, the addition of the χ_0 constraint to Eqs. (B5) will be denoted as $\text{DIP}_{\hat{\gamma}; \chi_0}^{(i)}$. It is by no means trivial that those new systems of constraints will have a solution at all. It crucially depends on the interpolator. In this respect, notice that the DIP ansatz has the right kinematics to comply with Eq. (73), which is highly nontrivial.

The results are shown in the last three lines of Table IV, where we scanned the solution over a wide interval for χ_0 , mostly covering all the values quoted in the literature so far. The range for χ_0 is indicated in each case. While, in principle, we took $0 \leq \chi_0 \leq 8.9 \text{ GeV}^{-2}$, wherever the interval is shorter, it means that no solution was available beyond that point. In particular, $\text{DIP}_{\hat{\gamma}; \chi_0}^{(1)}$ gave no solution at all in the full interval.

Taken at face value, the results of Table IV indicate a potential (10 – 15)% effect due to the our

Model	$w_1 G_1$	$w_2 G_2$	$w_3 G_3$	$w_4 G_4$	a_μ
DIP $_{\hat{\alpha}}$	+0.018(3)	+0.034(4)	+0.0016	-0.0002	$6.7(3) \cdot 10^{-10}$
DIP $_{\hat{\beta}; m_2=m_\rho}^{(1)}$	+0.014	+0.037	+0.0015	-0.0002	$6.52(15)(10) \cdot 10^{-10}$
DIP $_{\hat{\beta}; m_2=m_\rho}^{(2)}$	+0.014	+0.037	+0.0015	-0.0002	$6.55(21)(6) \cdot 10^{-10}$
DIP $_{\hat{\gamma}; m_2=m_\rho}^{(1)}$	+0.004	+0.047	+0.0015	-0.0002	$6.09(81)(9) \cdot 10^{-10}$
DIP $_{\hat{\gamma}; m_2=m_\rho}^{(2)}$	+0.002	+0.047	+0.0015	-0.0002	$6.21(77)(7) \cdot 10^{-10}$
DIP $_{\hat{\beta}; 0 < \chi_0 < 8.9}^{(1)}$	[+0.003; +0.047]	[+0.043; +0.022]	[+0.0015; +0.0016]	-0.0002	$[5.9; 8.9] \cdot 10^{-10}$
DIP $_{\hat{\beta}; 0 < \chi_0 < 4.4}^{(2)}$	[+0.002; +0.027]	[+0.044; +0.025]	+0.0015	-0.0002	$[6.0; 6.7] \cdot 10^{-10}$
DIP $_{\hat{\gamma}; 0 < \chi_0 \leq 6.4}^{(2)}$	[+0.006; +0.035]	[+0.043; +0.022]	[+0.0015; +0.0016]	-0.0002	$[6.3; 7.3] \cdot 10^{-10}$

TABLE IV: Determination of a_μ with the generalized DIP parametrizations and their comparison with the DIP $_{\hat{\alpha}}$ model. We explicitly show the contribution from the different generalized form factors G_i . The errors in parentheses are the ones induced by $\hat{\alpha}$ followed by $\hat{\beta}$ or $\hat{\gamma}$. For the last 3 rows, where χ_0 is inside a range, we show the values for the endpoints.

Model	$\hat{\alpha}$ (GeV $^{-2}$)	$\hat{\beta}$ (GeV $^{-4}$)	$\hat{\gamma}$ (GeV $^{-4}$)	χ_0 (GeV $^{-2}$)
DIP $_{\hat{\alpha}}$	-1.76*	2.67	4.25	2.42
DIP $_{m_\rho}$	-1.35	1.73	2.25	1.66
DIP $_{\hat{\beta}; m_2=m_\rho}^{(1)}$	-1.76*	3.33*	3.78	1.61
DIP $_{\hat{\beta}; m_2=m_\rho}^{(2)}$	-1.76*	3.33*	3.88	1.69
DIP $_{\hat{\gamma}; m_2=m_\rho}^{(1)}$	-1.76*	4.56	2.84*	-0.81
DIP $_{\hat{\gamma}; m_2=m_\rho}^{(2)}$	-1.76*	5.23	2.84*	-0.74
DIP $_{\hat{\beta}; 0 < \chi_0 < 8.9}^{(1)}$	-1.76*	3.33*	[3.10; $-5 \cdot 10^5$]	[0; 8.9]*
DIP $_{\hat{\beta}; 0 < \chi_0 < 4.4}^{(2)}$	-1.76*	3.33*	[3.19; -3.18]	[0; 4.4]*
DIP $_{\hat{\gamma}; 0 < \chi_0 \leq 6.4}^{(2)}$	-1.76*	[5.47, -18]	2.84*	[0; 6.4]*

TABLE V: Predicted low-energy parameters from the different parametrizations. Asterisk quantities are input of the different DIP interpolators. For the last 3 rows, where χ_0 is inside a range, we show the values for the endpoints. Notice from the last three lines that large values for χ_0 are clearly disfavored.

present knowledge of the parameter χ_0 . The way to read this result is that the off-shellness of the pion can induce, at most, a 15% shift on values obtained within the pion-pole approximation. While the uncertainty on χ_0 can only be reduced with a reliable calculation (probably from the lattice), we can still investigate which are the preferred values for χ_0 for the different interpolators we have been dealing with. The results are collected in Table V. Notice that lower values for χ_0 are preferred (first six rows). In contrast, large values for χ_0 give wrong

predictions for the low-energy parameters (see the last 3 rows) and hence they are clearly disfavored. While this might be indicative, it is certainly not conclusive. It is therefore essential to have a better understanding of χ_0 . Incidentally, Table V also shows that DIP $_{\hat{\gamma}}^{(1,2)}$ predicts not only slightly large values for $\hat{\beta}$ but also negative central values for χ_0 . This seems to confirm that the results of DIP $_{\hat{\gamma}}^{(1,2)}$ might be unreliable.

-
- [1] G. W. Bennett *et al.* [Muon g-2 Collaboration], Phys. Rev. Lett. **92**, 161802 (2004) [arXiv:hep-ex/0401008].
 - [2] J. Bijnens, E. Pallante and J. Prades, Nucl. Phys. B **626**, 410 (2002) [arXiv:hep-ph/0112255].
 - [3] M. Hayakawa and T. Kinoshita, Phys. Rev. D **57**, 465 (1998) [Erratum-ibid. D **66**, 019902 (2002)] [arXiv:hep-ph/9708227].
 - [4] M. Knecht and A. Nyffeler, Phys. Rev. D **65**, 073034 (2002) [arXiv:hep-ph/0111058].
 - [5] K. Melnikov and A. Vainshtein, Phys. Rev. D **70**, 113006 (2004) [arXiv:hep-ph/0312226].
 - [6] A. Nyffeler, Phys. Rev. D **79**, 073012 (2009) [arXiv:0901.1172 [hep-ph]].
 - [7] M. Knecht, A. Nyffeler, M. Perrottet and E. de Rafael, Phys. Rev. Lett. **88**, 071802 (2002)

- [arXiv:hep-ph/0111059].
- [8] A. Nyffeler, arXiv:1001.3970 [Unknown].
 - [9] R. M. Carey *et al.*, FERMILAB-PROPOSAL-0989.
 - [10] J. Imazato, Nucl. Phys. Proc. Suppl. **129**, 81 (2004).
 - [11] D. Babusci *et al.*, arXiv:1007.5219 [Unknown].
 - [12] J. Prades, E. de Rafael and A. Vainshtein, arXiv:0901.0306 [hep-ph].
 - [13] F. Jegerlehner and A. Nyffeler, Phys. Rept. **477**, 1 (2009) [arXiv:0902.3360 [hep-ph]].
 - [14] J. M. Maldacena, Adv. Theor. Math. Phys. **2**, 231 (1998) [Int. J. Theor. Phys. **38**, 1113 (1999)];
 - [15] G. Isidori, *Physics motivations for off-peak physics*, talk given at the *KLOE2 Physics Workshop 09*.
 - [16] H. J. Behrend *et al.* [CELLO Collaboration], Z. Phys. C **49**, 401 (1991).
 - [17] J. Bijnens and F. Perrsson, arXiv:hep-ph/0106130.
 - [18] G. D'Ambrosio, G. Isidori and J. Portoles, Phys. Lett. B **423**, 385 (1998) [arXiv:hep-ph/9708326].
 - [19] I. R. Klebanov and E. Witten, Nucl. Phys. B **556**, 89 (1999) [arXiv:hep-th/9905104].
 - [20] J. Erlich, E. Katz, D. T. Son and M. A. Stephanov, Phys. Rev. Lett. **95**, 261602 (2005)
 - [21] L. Da Rold and A. Pomarol, Nucl. Phys. B **721**, 79 (2005);
 - [22] T. Sakai and S. Sugimoto, Prog. Theor. Phys. **113**, 843 (2005);
 - [23] T. Sakai and S. Sugimoto, Prog. Theor. Phys. **114**, 1083 (2005)
 - [24] J. Hirn and V. Sanz, JHEP **0512**, 030 (2005);
 - [25] A. Karch, E. Katz, D. T. Son and M. A. Stephanov, Phys. Rev. D **74**, 015005 (2006)
 - [26] S. S. Gubser, I. R. Klebanov and A. M. Polyakov, Phys. Lett. B **428**, 105 (1998);
 - [27] E. Witten, Adv. Theor. Math. Phys. **2**, 253 (1998)
 - [28] C. T. Hill, Phys. Rev. D **73**, 126009 (2006).
 - [29] M. Gell-Mann, R. J. Oakes and B. Renner, Phys. Rev. **175**, 2195 (1968).
 - [30] E. Witten, Adv. Theor. Math. Phys. **2**, 505 (1998) [arXiv:hep-th/9803131].
 - [31] H. R. Grigoryan and A. V. Radyushkin, Phys. Rev. D **76**, 095007 (2007).
 - [32] H. R. Grigoryan and A. V. Radyushkin, Phys. Rev. D **77**, 115024 (2008) [arXiv:0803.1143 [hep-ph]].
 - [33] H. R. Grigoryan and A. V. Radyushkin, Phys. Rev. D **76**, 115007 (2007).
 - [34] H. R. Grigoryan and A. V. Radyushkin, Phys. Rev. D **78**, 115008 (2008) [arXiv:0808.1243 [hep-ph]].
 - [35] G. P. Lepage and S. J. Brodsky, Phys. Rev. D **22**, 2157 (1980).
 - [36] S. J. Brodsky and G. P. Lepage, Phys. Rev. D **24**, 1808 (1981).
 - [37] J. Gronberg *et al.* [CLEO Collaboration], Phys. Rev. D **57**, 33 (1998) [arXiv:hep-ex/9707031].
 - [38] B. Aubert *et al.* [The BABAR Collaboration], Phys. Rev. D **80**, 052002 (2009) [arXiv:0905.4778 [hep-ex]].
 - [39] M. F. L. Golterman and S. Peris, Phys. Rev. D **61**, 034018 (2000) [arXiv:hep-ph/9908252].
 - [40] M. Knecht and A. Nyffeler, Eur. Phys. J. C **21**, 659 (2001) [arXiv:hep-ph/0106034].
 - [41] C. Amsler *et al.* (Particle Data Group), Phys. Lett. B **667**, 1 (2008) and 2009 partial update for the 2010 edition.
 - [42] D. K. Hong and D. Kim, Phys. Lett. B **680**, 480 (2009) [arXiv:0904.4042 [hep-ph]].
 - [43] F. Jegerlehner, Acta Phys. Polon. B **38**, 3021 (2007) [arXiv:hep-ph/0703125].
 - [44] A. E. Dorokhov and W. Broniowski, Phys. Rev. D **78**, 073011 (2008) [arXiv:0805.0760 [hep-ph]].
 - [45] P. Ball, V. M. Braun and N. Kivel, Nucl. Phys. B **649**, 263 (2003) [arXiv:hep-ph/0207307].
 - [46] J. Rohrwild, JHEP **0709**, 073 (2007) [arXiv:0708.1405 [hep-ph]].
 - [47] A. Vainshtein, Phys. Lett. B **569**, 187 (2003) [arXiv:hep-ph/0212231].
 - [48] A. Gorsky and A. Krikun, Phys. Rev. D **79**, 086015 (2009) [arXiv:0902.1832 [hep-ph]].
 - [49] O. Cata, Phys. Rev. D **81**, 054011 (2010) [arXiv:0911.4736 [Unknown]].
 - [50] B. L. Ioffe and A. V. Smilga, Nucl. Phys. B **232**, 109 (1984).
 - [51] L. Cappiello, O. Cata and G. D'Ambrosio, arXiv:1004.2497 [Unknown].
 - [52] O. Cata and V. Mateu, JHEP **0709**, 078 (2007) [arXiv:0705.2948 [hep-ph]].